Journal of Alloys and Compounds 685 (2016) 454–458

Contents lists available at ScienceDirect

Journal of Alloys and Compounds

journal homepage: http://www.elsevier.com/locate/jalcom

Anomalous Hall effect in $Co_{40}Fe_{40}B_{20}/SiO_2/Si$ structures

Y. Zhang, W.B. Mi*

Tianjin Key Laboratory of Low Dimensional Materials Physics and Preparation Technology, Faculty of Science, Tianjin University, Tianjin 300072, China

A R T I C L E I N F O

Article history:
Received 2 May 2016
Received in revised form
15 May 2016
Accepted 19 May 2016
Available online 31 May 2016

Keywords:
Anomalous Hall effect
Semiconductor
$Co_{40}Fe_{40}B_{20}$

A B S T R A C T

$Co_{40}Fe_{40}B_{20}/SiO_2/Si$ structures fabricated by a facing-target sputtering method exhibit anomalous Hall effect. The longitudinal resistance shows a metal-insulator transition with the increase of temperature. The Hall resistance first increases, and then decreases with the increase of temperature. The character of Hall loops undergoes a crossover from AHE to ordinary Hall effect with the increase of temperature. Such electronic transport properties can be understood by a two current channels model. On the other hand, the critical saturated magnetic field of Hall loops drops rapidly at 350 K, which can be attributed to the reduction of spin-polarized carriers in $Co_{40}Fe_{40}B_{20}$.

1. Introduction

Anomalous Hall effect (AHE) has received intense renewed interest in recently years due to its fundamental physics related to spin-dependent transport and technical applications in field sensors [1,2]. Ferromagnetic metals and alloys were mostly used for the research [2–4]. Magnetic granular films exhibit giant Hall resistivity [5]. The contributions of surface and interface scattering on AHE were also verified in ferromagnetic/nonmagnetic (FM/NM) multilayers, such as $[Co/Pd]_n$, $[Co/Cu]_n$ and $[Co/Pt]_n$ [6–8]. The effect of FM/FM interface on AHE was studied in $[Co/Ni]_n$ structures [9]. The AHE in ferromagnet/semiconductor (FM/SC) structures was also reported in Fe/Si, Fe/Ge and Fe/GaAs [10–12]. Compared with the extensively studied AHE in magnetic materials, little effort is made to investigate the AHE in $FM/SiO_2/Si$ structures focusing on the shunting effect from Si. The $FM/SiO_2/Si$ is one of the most widely used structures for spin injection into Si in semiconductor spintronics because of Si with weaker spin-orbit coupling and of SiO_2 buffer layer which can reduce the reaction and conductivity mismatch between FM layer and Si substrate [13,14]. Furthermore, the effect of carriers transporting between FM and Si on the AHE has been neglected. No-monotonic dependence of AHE resistivity on temperature was found in Fe/Gd bilayers [15]. The AHE was found not to follow the scaling law derived from skew scattering or side jump mechanisms in Fe/Cu bilayers [16]. Such unconventional phenomena arise from the carriers transporting between Fe and Gd (Cu) layers [15,16]. Therefore, it is interesting to investigate the AHE in $FM/SiO_2/Si$ structures, especially, with the presence of carriers transporting between FM and Si.

$Co_{40}Fe_{40}B_{20}$ films are widely used ferromagnetic material in spintronics, which have been intensively studied for its use in magnetic tunnel junctions [17] and spin transfer torque devices [18]. Su et al. have studied the proper scaling of AHE in $Co_{40}Fe_{40}B_{20}$ films [19]. Zhu et al. have interpreted the AHE in $MgO/Co_{40}Fe_{40}B_{20}/Ta$ and $Ta/Co_{40}Fe_{40}B_{20}/MgO$ structures [20,21]. However, the AHE in $Co_{40}Fe_{40}B_{20}/SiO_2/Si$ structures, which is of possible application in future spin-based devices [13,14,22], is not reported yet. In this letter, we investigate the AHE in $Co_{40}Fe_{40}B_{20}/SiO_2/Si$ structures. The AHE in $Co_{40}Fe_{40}B_{20}/SiO_2/Si$ structures is distinctly different from previously reported results on $Co_{40}Fe_{40}B_{40}$ films. The longitudinal and AHE resistance of $Co_{40}Fe_{40}B_{20}/SiO_2/Si$ structures first increase, and then decrease with the increase of temperature showing a metal-insulator transition. The character of Hall loops of $Co_{40}Fe_{40}B_{20}/SiO_2/Si$ structures undergoes four different stages with the increase of temperature. A two current channels model has been proposed to interpret the AHE in $Co_{40}Fe_{40}B_{20}/SiO_2/Si$ structures. The critical saturated magnetic field of Hall loops drops rapidly at 350 K, which is related to the reduction of spin-polarized carriers in $Co_{40}Fe_{40}B_{20}$ layer.

2. Experiment

$Co_{40}Fe_{40}B_{20}$ films were grown by dc facing-target sputtering from a pair of $Co_{40}Fe_{40}B_{20}$ targets on nature-oxidized *n*-type Si(100) and glass substrates at room temperature. The facing-target

* Corresponding author.
E-mail address: miwenbo@tju.edu.cn (W.B. Mi).

http://dx.doi.org/10.1016/j.jallcom.2016.05.339

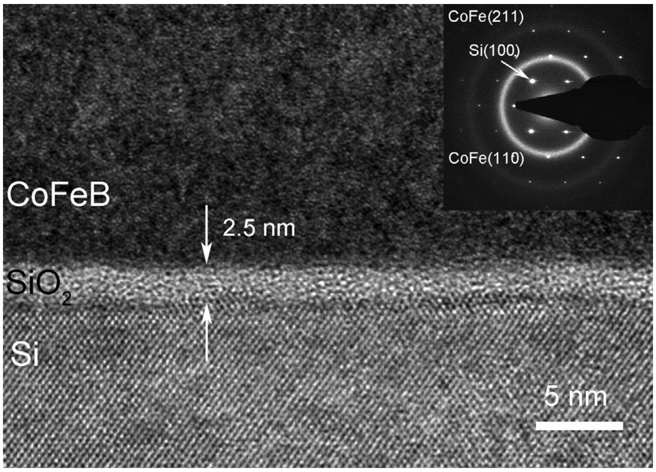

Fig. 1. High-resolution cross-section TEM image of $Co_{40}Fe_{40}B_{20}$ film on Si(100) substrate, the inset is the selected-area electron diffraction patterns.

method can suppress interaction between $Co_{40}Fe_{40}B_{20}$ film and Si substrate across SiO_2 layer because the substrate was free from the bombardment of high-energy particles during sputtering. The thickness (t) of Si substrate was about 500 μm and its resistivity is 0.03 Ω cm (doping density of 6×10^{17} cm^{-3}). The magnetizations of samples were measured by a Quantum Design superconducting quantum interference device. The electronic transport properties were measured by a Quantum Design physical property measurement system (PPMS-9) in the temperature range of 5–375 K. Hall bars were fabricated by using the shadow masks that have five terminals, which can be used to measure transverse and longitudinal resistances simultaneously. For excluding the contact resistance, the real Hall resistivity was obtained by subtracting the Hall resistivity measured at the negative magnetic fields from that measured at the positive magnetic fields, then divided by 2 because the magnetoresistance is an even function of magnetic field.

3. Result and discussion

Fig. 1 shows the cross-sectional high-resolution transmission electron microscopy (HRTEM) image of $Co_{40}Fe_{40}B_{20}$ film with $t = 160$ nm on nature-oxided Si substrate. The HRTEM micrograph gives a clear view of the $Co_{40}Fe_{40}B_{20}/SiO_2/Si$ structure. The interface on either side of SiO_2 is clean and sharp. The SiO_2 layer is 2.5 nm thick. The lattice fringes of Si substrate can be clearly observed, but no lattice fringes from $Co_{40}Fe_{40}B_{20}$ appear. From the selected-area electron diffraction patterns as shown in the insert of Fig. 1, we can see that a broad holo from amorphous $Co_{40}Fe_{40}B_{20}$ appears and the other spot patterns come from single-crystal Si(100). The broad ring appears from randomly orientated small crystallites CoFe(110) and CoFe(211), indicating that the sample has only short-range order at the atomic length scale. The bright-field HRTEM image and selected-area electron diffraction patterns suggest that the as-deposited $Co_{40}Fe_{40}B_{20}$ films are amorphous.

Fig. 2a shows the longitudinal resistance (R) as a function of temperature for $Co_{40}Fe_{40}B_{20}/SiO_2/Si$ structures with $t = 40$ and 160 nm. The temperature-dependent R is distinctly different from that of amorphous $Co_{40}Fe_{40}B_{20}$ films reported in literatures [23]. R decreases sharply at high temperature regions, which shows a semiconducting-like characteristic. An obvious metal-insulator transition of samples with the increase of temperature can be observed as shown in the top and bottom inserts of Fig. 2a. In our previous work, the amorphous $Co_{40}Fe_{40}B_{20}$ films with $t = 40$, 160 nm grown on glass substrates show a metallic behavior in the temperature range from 100 to 300 K [24]. The R-T curves of $Co_{40}Fe_{40}B_{20}/SiO_2/Si$ structures suggest that Si substrate plays an important role on the electrical transport properties. Similar

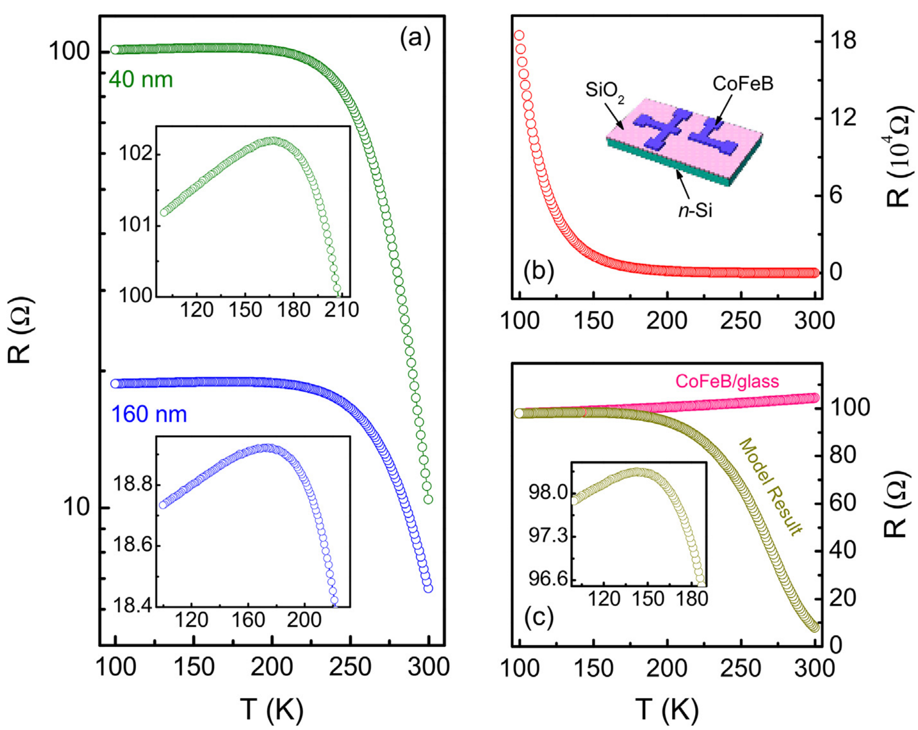

Fig. 2. (a) Temperature dependence of R of $Co_{40}Fe_{40}B_{20}/SiO_2/Si$ structures with $t = 40$ and 160 nm. The top and bottom inserts illustrate the enlarge graphs respectively. (b) Temperature dependence of R of $Co_{40}Fe_{40}B_{20}/SiO_2/Si$ structure with a middle gap. Insert: the schematic illustration of the sample with a middle gap. (c) The R-T curves of $Co_{40}Fe_{40}B_{20}$/glass structure and model result. Insert: the enlarge graph for model result.